Coherent backscattering of light in the presence of time-reversal-noninvariant and parity-nonconserving media

F. C. MacKintosh and Sajeev John
Physics Department, Princeton University, P.O. Box 708, Princeton, New Jersey 08544
(Received 26 May 1987)

We describe theoretically how the shape of the coherent backscattering peak of photons in a disordered dielectric medium is altered by Faraday rotation and natural optical activity. These effects break time-reversal and parity symmetries, respectively. The calculated line shapes are qualitatively similar to those in the presence of confined geometry or in an absorptive medium: The suppression of long scattering paths reduces the observed peak intensity. For incident light of a given circular polarization, however, Faraday rotation suppresses only backscattered light of the same helicity, whereas optical activity suppresses coherence in the opposite helicity channel and leaves the helicity-preserving channel unaffected. It is shown that the helicity-preserving component of the backscattered peak for electromagnetic waves is quantitatively similar to the peak calculated for scalar waves. This correspondence remains as a function of slab thickness and absorption, in agreement with recent experiments. In contrast, the peak line shapes for linearly polarized incident light exhibit quantitative differences in either linear polarization channel from scalar waves. These results were obtained in the diffusion approximation, and for an uncorrelated random medium.

I. INTRODUCTION

There has been much interest recently in the transport properties of classical waves, such as light, in strongly scattering disordered media. This interest has been motivated in part by the question of whether Anderson localization of photons may be observed in such systems.[1,2] So far only *weak* localization of light has been conclusively observed in the phenomenon of coherent backscattering.[3–7] This phenomenon has been discussed in the context of electron localization by Khmel'nitskii[8] and developed further by Bergmann.[9] It is the precursor to true Anderson (*strong*) localization and gives rise to the renormalization of the energy diffusion coefficient for waves in a random medium as described by the scaling theory of localization.[10] Optical systems provide a unique opportunity for the direct experimental observation of this effect. Golubentsev[11] has considered the albedo for retroreflectance of scalar waves from a random collection of pointlike scattering centers. Akkermans, Wolf, and Maynard[12] have extended these ideas to obtain the actual line shape of coherent backscattering of scalar waves from a disordered dielectric half-space. Although the vector nature of the electromagnetic field does not alter the localization critical point, polarization effects are apparent in angle resolved studies of the backscattering intensity.[3–5] Stephen and Cwilich[13] have shown that for linearly polarized light incident on a scattering medium, the backscattering peak consists of a sharp narrow peak polarized parallel to the incident light as well as a broader depolarized peak. This agrees with recent experiments.[4,14,15] It is the purpose of this paper to recapture these formal results by means of simple physical arguments and to extend them to systems in which time reversal and parity symmetries are broken. These include magneto-optically active materials in which this broken symmetry is manifest in unequal propagation speed for right- and left-circularly-polarized light parallel to a magnetic field. This is the familiar Faraday effect. Qualitatively, the effect of broken time-reversal symmetry is to round off the peak in the backscattering intensity due to the removal of long diffusion paths from the coherent intensity. In particular, we find that this decreases primarily the peak intensity of the helicity preserving component of the backscattering signal. For incident light of a given circular polarization, it is the scattered light of the same circular polarization which is suppressed. An *in situ* monitoring of this cutoff in interfering diffusion paths as a function of external field would be of particular interest near the mobility edge where the absence of time-reversal symmetry can lead to new critical exponents for the localization transition.

A less severe form of broken symmetry arises in naturally optically active materials in which right- and left-circularly-polarized photons experience different dielectric constants independent of their direction of propagation. In such materials time-reversal symmetry is maintained and the helicity-preserving component of the backscattering peak remains unaffected. The breakdown of parity, however, leads to a decrease in the opposite helicity portion of the intensity.

In this paper we consider only the leading correction to the classical diffusion propagator. In perturbation theory, ordinary diffusion comes from the sum of *ladder* diagrams, whereas the leading correction corresponds to

the sum of the *maximally crossed* diagrams. This second sum gives rise to a backscattering peak with angular width proportional to the small parameter $\lambda/2\pi l$, where λ is the wavelength and l is the mean free path. In Sec. II we present a simple physical picture of the effects of broken time-reversal symmetry and parity nonconservation on this peak line shape. In Secs. III and IV these arguments are supported by a detailed derivation of the relevant Green's functions.

II. THE PHYSICAL PICTURE

The classical multiple-scattering treatment of wave propagation ignores phase correlation on length scales longer than the mean free path l. For elastic scattering in macroscopic samples this treatment yields the diffusion equation with constant $D=lc/3$, where c is the wave velocity. For weak scattering ($l \gg \lambda$) this approximation is good except in the backward direction, where phase correlation of even long paths cannot be ignored. A variety of authors have discussed the significance of this interference.[12,16] Consider a half-space of randomly placed scatterers and a typical path γ shown as the solid line in Fig. 1(a). Incident light with wave vector $\mathbf{k}_i=\mathbf{k}_0$ is scattered at points $\mathbf{x}_1, \ldots, \mathbf{x}_N$ ($N>1$) into intermediate states with wave vectors $\mathbf{k}_1, \ldots, \mathbf{k}_{N-1}$, and, finally, to the state $\mathbf{k}_N=\mathbf{k}_f$. For scalar waves undergoing an identical set of wave-vector transfers, the scattering amplitudes at the points $\mathbf{x}_1, \ldots, \mathbf{x}_N$ are the same for the path γ and the time-reversed path $-\gamma$ (the dashed line). The nature of the interference between these paths is determined solely by their relative optical path lengths—thus the relative phase is $e^{i(\mathbf{k}_i+\mathbf{k}_i)\cdot(\mathbf{x}_N-\mathbf{x}_1)}$. For strict backward scattering ($\mathbf{q}=\mathbf{k}_i+\mathbf{k}_f=0$), the amplitudes for the two paths are equal ($A_\gamma=A_{-\gamma}$) and hence the intensity will have a contribution $\sim |A_\gamma+A_{-\gamma}|^2=4|A_\gamma|^2$, which is twice the contribution $\sim |A_\gamma|^2+|A_{-\gamma}|^2$ obtained when correlation is ignored. Thus a peak of height twice the classical result is obtained in the backward direction.

We may also see that the angular width of this peak should be roughly $\Delta\theta\sim(\lambda/2\pi l)$ since, for a larger angle θ, the argument of the phase $\mathbf{q}\cdot(\mathbf{x}_n-\mathbf{x}_1)$ is greater than $(2\pi/\lambda)\theta l \gtrsim 1$. Consider the case of a wave incident normal to the interface and $\mathbf{x}_N-\mathbf{x}_1$ parallel to the interface. If the angle between $-\mathbf{k}_i$ and $\mathbf{k}_f$ is θ, then the coherence condition for small θ becomes $\mathbf{q}\cdot(\mathbf{x}_N-\mathbf{x}_1)=2\pi\theta|\mathbf{x}_N-\mathbf{x}_1|/\lambda<1$. In the diffusion approximation $|\mathbf{x}_N-\mathbf{x}_1|^2\simeq D(t_N-t_1)\simeq lL/3$, where L is the total length of path γ. Thus typical paths of length L contribute only for angles less than $\theta_m=\lambda/(2\pi\sqrt{lL/3})$. To facilitate a generalization to a propagating vector field it is useful to look at this in another way. Consider the path in k space shown in Fig. 1(b), with wave-vector transfers $\mathbf{g}_j=\mathbf{k}_j-\mathbf{k}_{j-1}$ ($j=1, \ldots, N$). The reversed path is given by the transfers $\mathbf{g}_j$ in the reverse order: $\mathbf{g}_N, \ldots, \mathbf{g}_1$. The intermediate states no longer lie on the energy shell which is smeared by an amount $\hbar/\tau$, where $\tau=l/c$ is the mean lifetime of a plane wave in the disordered medium. For small $\mathbf{q}$, corresponding intermediate states differ in energy by an amount $E_{N-j}-E'_j\simeq c\hbar\mathbf{q}\cdot\hat{\mathbf{k}}_{N-j}$ ($j=1, \ldots, N-1$), where $\hat{\mathbf{k}}_{N-j}$ are unit vectors in the direction of propagation of the intermediate plane-wave states. The phase difference $\Delta\phi$ between paths is then

$$\Delta\phi=\sum_{j=1}^{N-1} c\tau_j\mathbf{q}\cdot\hat{\mathbf{k}}_j\simeq ql\sum_{j=1}^{N-1}\cos\theta_j\ , \tag{2.1}$$

where τ_j is the lifetime of the plane-wave state j. The values of $\cos\theta$ are random, and hence the sum corresponds to a random walk. After averaging over all possible N step walks, the root-mean-square (rms) phase difference $(\Delta\phi)_{\rm rms}$ is approximately $\sqrt{1/3Nql}$, and the condition for coherence is the same as above (with

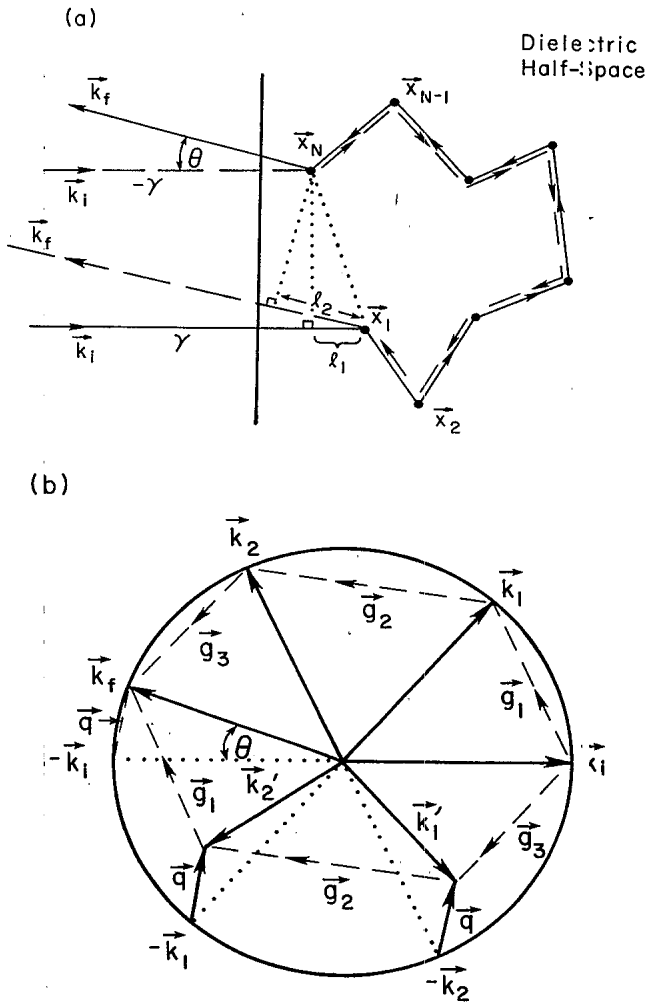

FIG. 1. (a) A typical scattering path (γ) in real space and the time reverse ($-\gamma$) with which it coherently interferes for small θ. The phase difference between γ and $-\gamma$ is simply proportional to the path length difference l_2-l_1, where $l_1=(\mathbf{x}_1-\mathbf{x}_N)\cdot\hat{\mathbf{k}}_i$ and $l_2=(\mathbf{x}_N-\mathbf{x}_1)\cdot\hat{\mathbf{k}}_f$. (b) A typical path drawn in momentum space. Equality of the scattering amplitudes requires that the wave-vector transfers $\mathbf{g}_j$ be the same but in the reverse order for the time-reversed path. Corresponding states differ in energy by an amount $E_{N-j}-E'_j\cong c\hbar\mathbf{q}\cdot\hat{\mathbf{k}}_j$, which leads to a phase difference $(\Delta\phi)_{\rm rms}\cong\sqrt{N/3}ql$.

$L \simeq Nl$). In particular, the observed cusp near $\theta=0$ depends on paths of arbitrary length. We thus expect that if coherence were limited to paths shorter than some maximum L_m, then the peak should be rounded off for angles less than $\lambda/(2\pi\sqrt{lL_m/3})$. Each of the symmetry-breaking effects considered below corresponds qualitatively to such a path length cutoff.

One such example has been considered by Stephen and Cwilich[13,17] in which scattering is confined to a slab of finite thickness W. In this case paths of length greater than $L_m=3W^2/l$ would have an appreciable probability of diffusing through the slab and being transmitted. Hence, the portion of the reflected peak depending on paths longer than L_m would no longer be observed. The calculation to be described in Sec. III gives the line shapes shown in Fig. 2(a). These curves are consistent both with experiments[18] and with the qualitative arguments above. Small deviations from the calculated line shapes are expected for large angles and for very thin slabs, where only short random walks contribute.[19] This can be understood as a breakdown of the diffusion approximation for short paths (see Sec. III).

Consider now what happens in the presence of absorption. One would expect that only paths of length less than the inelastic mean free path l_i would contribute. This is similar to the finite geometry case above with the correspondence $W \leftrightarrow \xi \equiv (ll_i/3)^{1/2}$ [see Fig. 2(b)]. A subtle distinction between these two cases arises for large angles as can be seen in the calculated line shapes. Short paths will not reach the far side of the slab, but will still be somewhat attenuated by absorption. Thus in the first case, the curves for finite W approach very closely that of $W=\infty$ for sufficiently large angles—more so than the curves for finite ξ. The length ξ may be viewed as the mean depth into the medium which a photon diffuses before being absorbed. The value of this length may be found as follows. Diffusion in the presence of absorption is described by a momentum space propagator

$$\mathcal{D}(k,\omega) \equiv \frac{1}{D(k^2+1/\xi^2)-i\omega} , \tag{2.2}$$

the steady-state ($\omega=0$) transform of which is

$$\mathcal{D}(r) = \frac{e^{-|r|/\xi}}{4\pi D r} . \tag{2.3}$$

Hence ξ has the interpretation of the *mean penetration depth* described above. On the other hand, the time-dependent transform of Eq. (2.2) is

$$\mathcal{D}(r,t) = \frac{e^{-|r|^2/Dt}}{(4\pi Dt)^{3/2}} e^{-Dt/\xi^2} . \tag{2.4}$$

Thus a typical photon travels for a time $t_m \simeq \xi^2/D = 3\xi^2/lc$ before being absorbed. It follows that $l_i = 3\xi^2/l$ and $\xi = \sqrt{ll_i/3}$.

For a vector field propagating in a random medium, the condition that the optical path lengths be the same for reversed paths is necessary but no longer sufficient for constructive interference. For photons, scattering produces a sequence of rotations of the polarization vector, which simply ensure that the wave remains transverse. The properties of these rotations have been described by a number of authors.[4,5,12] We may describe these rotations of the polarization vectors $\hat{\mathbf{e}}_j$ by matrices M_{j+1} which are real and symmetric. A sequence of scattering events rotates $\hat{\mathbf{e}}_0$ by the product $M_N \cdots M_1$, and the reverse sequence by the product $M_1 \cdots M_N = (M_N \cdots M_1)^T$ for exact backward scattering. The matrices M_j do not commute for general $\mathbf{k}_j$ in three dimensions and only diagonal elements such as $\langle \hat{\mathbf{x}} | M_N \cdots M_1 | \hat{\mathbf{x}} \rangle = \langle \hat{\mathbf{x}} | M_1 \cdots M_N | \hat{\mathbf{x}} \rangle$ will remain

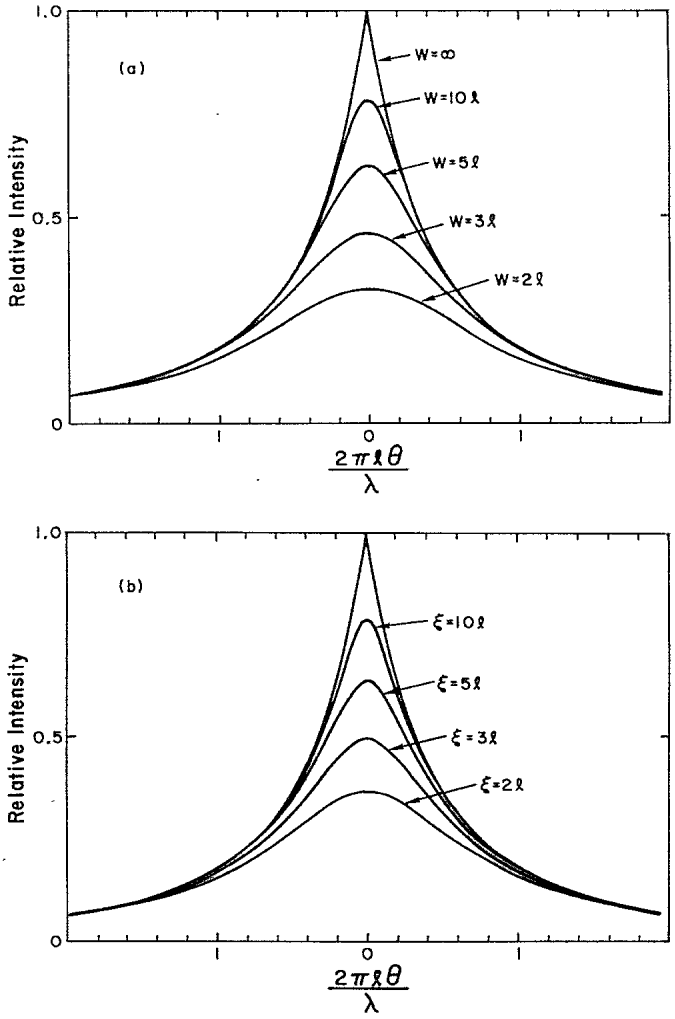

FIG. 2. The calculated scalar coherent backscattering line shapes. (a) As the width W of the scattering medium is reduced the central portion of the peak is suppressed by the termination of scattering paths. (b) Similarly the peak is reduced as absorption (with length l_i) is introduced. These curves are labeled by the mean penetration depth $\xi=(ll_i/3)^{1/2}$, which decreases with stronger absorption. Curves (a) and (b) are quite similar, with the correspondence $W \leftrightarrow \xi$. These curves represent the coherent peak, from which the isotropic background has been subtracted. The curves have then been normalized by the isotropic background intensity. Thus, the coherent peak of unit relative intensity corresponds to an actual enhancement factor of 2 in the total reflected intensity.

coherent. Thus backscattered light polarized parallel to the incident light will retain the sharp peak associated with long paths, while the perpendicular component will be suppressed. This suppression is apparent in the central part of the peak where long scattering sequences are important. The wings of the backscattering intensity, on the other hand, are dominated by shorter random walks where the noncommuting property of the rotation matrices is less serious. For example, backscattering from $\mathbf{k}_i$ to $-\mathbf{k}_i$ by an $N=2$ step process can always be drawn in a single plane. Since rotations in this plane commute, coherence is maintained. If one considers, rather, the scattering of circularly polarized states, the amplitudes relating incoming and outgoing right-hand R and left-hand L states involve phase factors which express the non-Abelian nature of the rotation group in three dimensions. For example, consider incident circularly-polarized light traveling along the $\hat{\mathbf{z}}$ axis which is scattered into a state along the axis $\hat{\mathbf{z}}'$ given by polar and azimuthal angles θ and ϕ. If we describe the outgoing states in the basis $\{\hat{\mathbf{x}}',\hat{\mathbf{y}}',\hat{\mathbf{z}}'\}$ obtained from the original basis by the rotation through angle θ about the axis parallel to $\hat{\mathbf{z}}\times\hat{\mathbf{z}}'$, then these amplitudes are given by the matrix

$$\begin{bmatrix} R' \\ L' \end{bmatrix} = \begin{bmatrix} \frac{1}{2}(1+\cos\theta) & \frac{1}{2}(\cos\theta-1)e^{-2i\phi} \\ \frac{1}{2}(\cos\theta-1)e^{2i\phi} & \frac{1}{2}(1+\cos\theta) \end{bmatrix} \begin{bmatrix} R \\ L \end{bmatrix} . \tag{2.5}$$

For an entering right-hand photon which executes a random walk and is backscattered into a left-hand helicity state there is a substantial reduction in the peak intensity due to the noncommutativity of these matrices. As in the case of parallel polarized light, however, the coherence of reversed paths is not destroyed for scattering into the same helicity state. This corresponds to the experimental configuration used to remove single-scattering events (which necessarily flip the helicity) from the observed intensity.[18] The incident light was circularly polarized and only scattered light of the same polarization was monitored. It should be noted that the backscattering peak in this channel closely resembles the calculated peak for scalar waves. [Compare Figs. 2(b) and 3(a) for example.] This similarity remains true in the presence of both confined geometry and absorption, for which we have also calculated the line shapes in the helicity-preserving channel. We also show in Sec. IV that due to the elimination of single-scattering contributions, the peak height in the helicity-preserving channel is exactly twice the (classical) isotropic background intensity—as is the case for scalar waves. In contrast, these similarities to the scalar line shapes do not hold in the parallel linearly polarized channel.[13]

Associated with the polarization of the electromagnetic field are additional effects which break time-reversal symmetry in the absence of dissipation. One of these is the Faraday effect. The origin of this effect can be seen in a simple classical picture. When subject to a circularly polarized electromagnetic wave, the bound electrons execute circular orbits. A strong magnetic field ($\mathbf{B}$) along the direction of the wave will introduce a radial force on the electron. Depending on the sense of polarization of the wave, the orbit will either be increased or decreased—changing the dipole moment of the electron. Thus the effective dielectric constants for the two polarizations will differ. It is known that the refractive indices for the two polarizations are given by $n_{R/L}\simeq n_0\mp\mathbf{g}\cdot\hat{\mathbf{k}}/2n_0$, where $\mathbf{k}$ is the wave vector, $\mathbf{g}=f\mathbf{B}$ is the gyration vector, and f is the Faraday constant.[20] Consider a path contributing to the helicity preserving channel (Fig. 4) with intermediate wave vectors $\mathbf{k}_j$ and helicities α_j ($+1$ for R and -1 for L), where for simplicity we have let $\mathbf{B}\propto\hat{\mathbf{k}}_i$. The helicities ($\alpha'_{N-j}=\alpha_j$) for

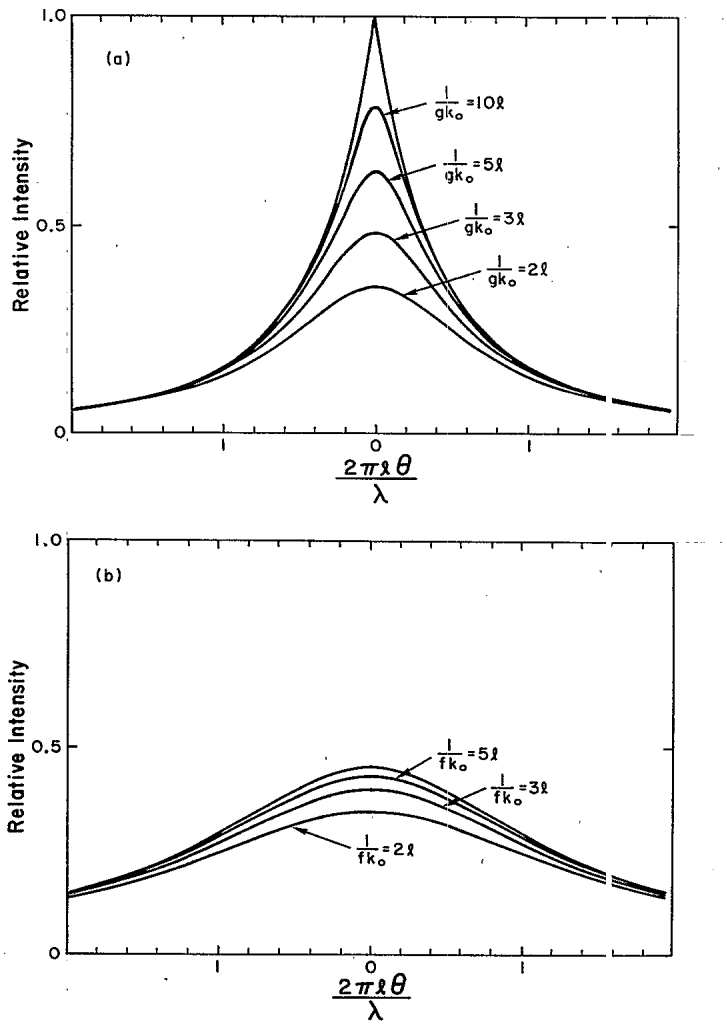

FIG. 3. (a) The effect of Faraday rotation on the peak line shape, where $\mathbf{g}=f\mathbf{B}$ is the gyration vector. The curves shown are for incident and reflected light of the same circular polarization. The opposite helicity channel is unaffected by Faraday rotation. (b) The suppression of the intensity in the opposite helicity channel due to natural optical activity. The gyration vector $\mathbf{g}=f\hat{\mathbf{k}}$ is proportional to the propagation direction. The helicity-preserving channel is unaffected since time-reversal symmetry is retained. Both curves have been normalized by the isotropic background intensity in the helicity-preserving channel.

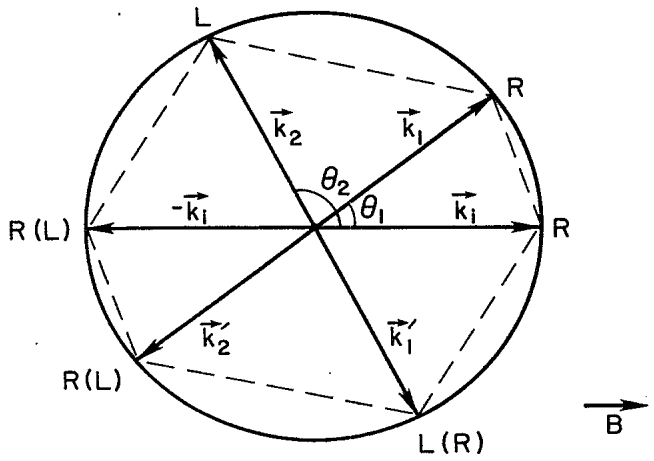

FIG. 4. Typical paths contributing to the two helicity channels. The helicities of the reversed path are labeled both for the Helicity-preserving channel as well as for the opposite helicity channel (in parentheses).

the reversed path are chosen such that the amplitudes of Eq. (2.5) associated with each momentum transfer are the same. There is, however, an optical path length difference between the two paths with the introduction of a magnetic field. This phase difference is

$$\Delta\phi = ck_0 \sum \tau_j \left[\alpha_j \frac{\mathbf{g}\cdot\hat{\mathbf{k}}_j}{2} - \alpha_j \frac{\mathbf{g}\cdot(-\hat{\mathbf{k}}_j)}{2} \right]$$

$$\simeq k_0 g l \sum \alpha_j \cos\theta_j \ , \tag{2.6}$$

where $k_0=\omega/c$. For large N, α_j, and $\cos\theta_j$ are uncorrelated. Hence, this is again a random-walk problem, so that $(\Delta\phi)_{\rm rms}\simeq k_0 g l[(1/3)N]^{1/2}$. Thus a magnetic field destroys coherence for such paths longer than $L_{\rm m}=1/l(k_0 g)^2$. This appears as a field-dependent rounding off of the backscattering peak. On the other hand, for paths related by $\mathbf{k}'_{N-j}=-\mathbf{k}_j$ and $\alpha'_{N-j}=-\alpha_j$ (helicities shown in parentheses in Fig. 4), the optical path lengths are the same. Hence, Faraday rotation does not affect the opposite helicity channel. As we shall show by a detailed derivation (Sec. IV), the effect of Faraday rotation on the helicity-preserving portion of the backscattering peak is similar to that of absorption with the correspondence $\xi \leftrightarrow 1/gk_0$. We also find that the reversed helicity channel is virtually unaffected by Faraday rotation, as the above argument suggests. The results of this calculation are shown in Fig. 3(a) for the helicity-preserving channel.

Natural optical activity provides a further example of a broken symmetry not previously considered in the context of localization: parity nonconservation. Microscopically there is a difference in the dielectric constants for the two helicity states due to the electromagnetic response of helical molecules within the medium.[21,22] In contrast with Faraday rotation, the dielectric constants are independent of the direction of propagation. Some examples of optically active media are sugar, turpentine, selenium, tellurium, $AgGaS_2$, TeO_2 and quartz. The induced dipole moment $\mathbf{p}=\alpha\mathbf{E}-\beta\mathbf{H}$ has the usual part proportional to the applied electric field $\mathbf{E}$ as well as a part opposite to the rate of change of the applied magnetic field $\mathbf{H}$. The latter contribution arises from electromotive forces in the helix given by Faraday's law of induction. The resulting constitutive relation for an optically active material yields an electric displacement vector $\mathbf{D}=\epsilon\mathbf{E}+i\mathbf{g}\times\mathbf{E}$, where $\mathbf{g}=f\hat{\mathbf{k}}$ is the gyration vector parallel to the direction of photon propagation. For small f, the refractive indices for right- and left-hand polarizations are $n_{R/L}\simeq n_0 \mp f/2n_0$. For the path shown in Fig. 4 in which $\alpha'_{N-j}=\alpha_j$, the optical path lengths for γ and $-\gamma$ are the same. Consequently, coherent backscattering into a helicity-preserving state is unaffected by natural optical activity. The same argument however does not hold for backscattering into a reversed helicity state, as in Fig. 4 with helicities shown in parentheses. In this latter case, we arrive at a phase difference $(\Delta\phi)_{\rm rms}\simeq k_0 f l[(1/3)N]^{1/2}$, which diminishes the backscattering intensity as the rotatory power f increases. This is illustrated in Fig. 3(b). We now proceed to derive the backscattering line shapes by evaluating the relevant photon Green's functions.

III. SCALAR WAVES: LINE SHAPES FOR CONFINED GEOMETRIES AND ABSORPTION

We begin by comparing the effects of confined geometries and absorption on the coherent backscattering of scalar waves. When the scattering medium is confined to a slab of finite width W, long diffusion paths can no longer contribute to the reflected intensity. Similarly, in an absorbing medium, paths longer than the inelastic mean free path l_i will be greatly attenuated. The peak line shapes for various slab thicknesses and for absorption are plotted in Figs. 2(a) and 2(b). We have extended the results of Stephen and Cwilich[13,23] to a larger variety of slab thicknesses and absorption coefficients. These curves were obtained by considering Green's functions for the scalar wave equation with source j:

$$\nabla^2\phi + \frac{\omega^2}{c^2}[\epsilon(\mathbf{r})\phi(\mathbf{r})] = j(\mathbf{r}) \ . \tag{3.1}$$

Here $\epsilon=1+\epsilon'+i\epsilon''$ is the dielectric constant, the real part of which fluctuates randomly about unity and the constant imaginary part leads to absorption with length $l_i=1/\epsilon''k_0$. For simplicity we consider a white-noise distribution for ϵ'

$$k_0^4\langle\epsilon'(\mathbf{r})\epsilon'(\mathbf{r}')\rangle_{\rm ensemble}=\gamma\delta^3(\mathbf{r}-\mathbf{r}') \ . \tag{3.2}$$

This is valid provided that the scale of the scattering microstructures is small compared with the wavelength of the excitation. Near a mobility edge, where these scales are expected to be comparable,[1] a more detailed analysis of the spatial correlations would be required. In the coherent potential approximation (CPA) and in the absence of dissipation ($\epsilon''=0$), the averaged Green's functions in the medium are given by the Fourier transforms

$$\langle G^{R/A}(k)\rangle=\frac{1}{k_0^2-k^2\pm ik_0/l}\ , \tag{3.3}$$

where $l=4\pi/\gamma$ is the elastic mean free path. Here the superscripts R and A denote retarded and advanced propagators, respectively. We have used the symbol $\langle\ \rangle$ in Eq. (3.3) and below to denote the average over all possible realizations of the disorder consistent with the statistics of Eq. (3.2). To simplify notation, explicit reference to this averaging of *single*-particle Green's functions will be omitted: In absence of the $\langle\ \rangle$ symbol, the Green's functions are to be interpreted as the single-particle averages given by Eq. (3.3). In an infinite medium, the Green's functions $G^{R/A}(\mathbf{r},\mathbf{r}')$ depend only on the spatial separation $(\mathbf{r}-\mathbf{r}')$, since the average over the disorder ϵ' restores translational symmetry. The coherent propagation of the field ϕ is described by the retarded Green's function

$$G^R(\mathbf{r}-\mathbf{r}')=\int\frac{d^3k}{(2\pi)^3}e^{i\mathbf{k}\cdot(\mathbf{r}-\mathbf{r}')}G^R(\mathbf{k})$$
$$=-\frac{\exp[(ik_0-1/2l)\,|\,\mathbf{r}-\mathbf{r}'\,|\,]}{4\pi\,|\,\mathbf{r}-\mathbf{r}'\,|} \tag{3.4}$$

with source j

$$\langle\phi(\mathbf{r})\rangle=\int d^3r'G^R(\mathbf{r}-\mathbf{r}')j(\mathbf{r}')\ . \tag{3.5}$$

The exponential decay of G reflects the fact that the plane-wave states have a finite lifetime $\tau=l/c$ due to elastic scattering. Hereafter, unless otherwise stated, we abbreviate the real-space and wave-vector integrals by $\int_{\mathbf{R}}\equiv\int d^3\mathbf{R}$ and $\int_{\mathbf{K}}\equiv\int d^3\mathbf{K}/(2\pi)^3$. The averaged intensity at $\mathbf{R}$ is then

$$I(\mathbf{R})\equiv\langle\phi(\mathbf{R})\phi^*(\mathbf{R})\rangle=\int_{\mathbf{R}_1,\mathbf{R}_2}\langle G^R(\mathbf{R},\mathbf{R}_1)G^A(\mathbf{R}_2,\mathbf{R})\rangle j(\mathbf{R}_1)j^*(\mathbf{R}_2)\ . \tag{3.6}$$

If ϕ describes a field propagating with wave vector $\mathbf{k}$, then $\phi(\mathbf{R}+\delta\mathbf{R})=\phi(\mathbf{R})e^{i\mathbf{k}\cdot\delta\mathbf{R}}$. Thus the specific intensity at $\mathbf{R}$ of radiation with wave vector $\mathbf{k}$ is given by

$$J(\mathbf{R},\mathbf{k})\equiv\int_{\mathbf{r}}e^{-i\mathbf{k}\cdot\mathbf{r}}\left\langle\phi\left[\mathbf{R}+\frac{\mathbf{r}}{2}\right]\phi^*\left[\mathbf{R}-\frac{\mathbf{r}}{2}\right]\right\rangle$$
$$=\int_{\mathbf{R}',\mathbf{r},\mathbf{r}',\mathbf{k}'}e^{-i\mathbf{k}\cdot\mathbf{r}}e^{i\mathbf{k}'\cdot\mathbf{r}'}\left\langle G^R\left[\mathbf{R}+\frac{\mathbf{r}}{2},\mathbf{R}'+\frac{\mathbf{r}'}{2}\right]G^A\left[\mathbf{R}'-\frac{\mathbf{r}'}{2},\mathbf{R}-\frac{\mathbf{r}}{2}\right]\right\rangle J^0(\mathbf{R}',\mathbf{k}')\ , \tag{3.7}$$

where J^0 is the incident specific intensity. [It is obtained from the product of sources $j(\mathbf{R}_1\equiv\mathbf{R}'+\mathbf{r}'/2)j^*(\mathbf{R}_2\equiv\mathbf{R}'-\mathbf{r}'/2)$ in Eq. (3.6) by transforming in the relative coordinate $\mathbf{r}'$, in the same way that J is obtained from the product $\phi\phi^*$ in the first line of Eq. (3.7).] This interpretation is valid in the case of weak scattering, for which $k_0\,|\,\mathbf{R}-\mathbf{R}'\,|\gg1$. The correlation $\Gamma\equiv\langle G^RG^A\rangle$ is the quantity which we must calculate. It is given in real space by the integral equation

$$\Gamma(\mathbf{R},\mathbf{R}',\mathbf{r},\mathbf{r}')=\left\langle G^R\left[\mathbf{R}+\frac{\mathbf{r}}{2},\mathbf{R}'+\frac{\mathbf{r}'}{2}\right]G^A\left[\mathbf{R}'-\frac{\mathbf{r}'}{2},\mathbf{R}-\frac{\mathbf{r}}{2}\right]\right\rangle$$
$$=\Gamma^0+\int_{\mathbf{R}_1,\mathbf{R}_2,\mathbf{r}_1,\mathbf{r}_2}\Gamma^0(\mathbf{R},\mathbf{R}_1,\mathbf{r},\mathbf{r}_1)\Lambda(\mathbf{R}_1,\mathbf{R}_2,\mathbf{r}_1,\mathbf{r}_2)\Gamma(\mathbf{R}_2,\mathbf{R}',\mathbf{r}_2,\mathbf{r}')\ , \tag{3.8}$$

where $\Gamma^0=\langle G^R\rangle\langle G^A\rangle$ is just the product of averaged Green's functions and describes the intensity of the coherent field. We approximate Γ in the integrand of Eq. (3.8) by this coherent part of the field. The correlation Γ is most easily calculated in momentum space. We perform the transformations indicated in Eq. (3.7) as well as a transformation in the separation $\mathbf{R}-\mathbf{R}'$

$$\Gamma(\mathbf{K},\mathbf{k},\mathbf{k}')=\int_{\mathbf{R}-\mathbf{R}',\mathbf{r},\mathbf{r}'}e^{-i\mathbf{K}\cdot(\mathbf{R}-\mathbf{R}')}e^{-i\mathbf{k}\cdot\mathbf{r}}e^{i\mathbf{k}'\cdot\mathbf{r}'}$$
$$\times\left\langle G^R\left[\mathbf{R}+\frac{\mathbf{r}}{2},\mathbf{R}'+\frac{\mathbf{r}'}{2}\right]\right.$$
$$\left.\times G^A\left[\mathbf{R}'-\frac{\mathbf{r}'}{2},\mathbf{R}-\frac{\mathbf{r}}{2}\right]\right\rangle\ . \tag{3.9}$$

The vertex $\Lambda(\mathbf{K},\mathbf{k},\mathbf{k}')$ may be approximated by the sum of ladder diagrams,[24] denoted by $L(\mathbf{K},\mathbf{k},\mathbf{k}')$. The sum of these diagrams may be written as a geometric series in the variable

$$Q(\mathbf{K})=\gamma\int_{\mathbf{q}}G^R\left[\mathbf{q}+\frac{\mathbf{K}}{2}\right]G^A\left[\mathbf{q}-\frac{\mathbf{K}}{2}\right]\simeq1-\tfrac{1}{4}l^2K^2\ . \tag{3.10}$$

This sum yields the diffusion propagator of Eq. (2.2) (without absorption)

$$L(\mathbf{K},\mathbf{k},\mathbf{k}')=\frac{\gamma}{1-Q(\mathbf{K})}=\frac{3\gamma}{l^2K^2}=\frac{\gamma}{\tau}\mathcal{D}(K,0)\ . \tag{3.11}$$

Keeping only terms quadratic in K in Eqs. (3.10) and (3.11) corresponds to the diffusion approximation. For short diffusion paths (or equivalently, for large K), this approximation will cease to be valid. Higher-order terms lead to small but observable corrections, for exam-

ple, at large angles in the backscattering peak.[19] For a time-reversal-invariant medium, the sum of maximally crossed diagrams (obtained from the ladder diagrams by a time-reversal operation[25]) is related to the ladder sum by

$$C(\mathbf{K},\mathbf{k},\mathbf{k}')=L(\mathbf{k}+\mathbf{k}',\mathbf{K}+\mathbf{k}-\mathbf{k}',\mathbf{K}-\mathbf{k}+\mathbf{k}') =\frac{3\gamma}{l^2(\mathbf{k}+\mathbf{k}')^2} . \tag{3.12}$$

For brevity, we will use $\mathbf{s}$ to denote $\mathbf{k}+\mathbf{k}'$ below. Whereas the specific intensity is isotropic in the classical diffusion approximation, the maximally crossed diagrams lead to a coherent contribution which is singular in the backward direction ($\mathbf{s}=\mathbf{k}+\mathbf{k}'\cong 0$). It is this singularity which leads to the sharp peak of height twice the classical incoherent intensity in the backward direction.

In recent experiments[3–7,14,15,18,26] what has been measured is the reflection from a half-space or slab of finite width W. This reflection is described by the specific intensity with wave-vector $\mathbf{k}_f$ exiting the medium at $\mathbf{R}$

$$J(\mathbf{R},\mathbf{k}_f)=\int_{\mathbf{R}_1,\mathbf{R}_2,\mathbf{k}_1,\mathbf{k}_2}\Gamma^0(\mathbf{R}-\mathbf{R}_1,\mathbf{k}_f,\mathbf{k}_1)[L(\mathbf{R}_1,\mathbf{R}_2,\mathbf{k}_1,\mathbf{k}_2)+C(\mathbf{R}_1,\mathbf{R}_2,\mathbf{k}_1,\mathbf{k}_2)]\int_{\mathbf{R}'\in S}\Gamma^0(\mathbf{R}_2-\mathbf{R}',\mathbf{k}_2,\mathbf{k}_i)J^0(\mathbf{R}',\mathbf{k}_i) , \tag{3.13}$$

where J^0 represents the light incident on the medium at $\mathbf{R}'$. For simplicity we have assumed a plane wave with wave-vector $\mathbf{k}_i$ incident on the surface of the medium. The integral over $\mathbf{R}'$ is restricted to this surface (S) and simply yields the coherent radiation at $\mathbf{R}_2$. This radiation is described by

$$\Gamma^0(\Delta,\mathbf{k}_1,\mathbf{k}_2)=\int_{\mathbf{r}_1,\mathbf{r}_2}e^{-i\mathbf{k}_1\cdot\mathbf{r}_1}e^{i\mathbf{k}_2\cdot\mathbf{r}_2}G^R\left[\mathbf{R}_1+\frac{\mathbf{r}_1}{2},\mathbf{R}_2+\frac{\mathbf{r}_2}{2}\right]G^A\left[\mathbf{R}_2-\frac{\mathbf{r}_2}{2},\mathbf{R}_1-\frac{\mathbf{r}_1}{2}\right] =\frac{e^{-|\Delta|/l}}{(4\pi|\Delta|)^2}(2\pi)^6\delta(\mathbf{k}_1-k_0\hat{\Delta})\delta(\mathbf{k}_2-k_0\hat{\Delta}) \tag{3.14}$$

in the approximation that $r_1,r_2\ll|\Delta|$, where $\Delta\equiv\mathbf{R}_1-\mathbf{R}_2$. The boundary conditions on the diffusion propagator $\mathcal{D}$ have been studied in various confined geometries in the context of classical transport theory.[27] It is known that for a semi-infinite medium of point scatterers, the propagator vanishes on a trapping plane located a distance $z_b\cong 0.7l$ outside of the medium. We have imposed this same condition at both boundaries of the slab. We may expect this to be valid only so long as the width $W\gg l$, since the diffusion approximation is not a good description of very short random walks, which will dominate for small W. Our calculations based on these boundary conditions, however, appear to be consistent with recent experiments[18] for widths as small as $W\cong 1.5l$. These boundary conditions may be satisfied by the familiar method of images, e.g., $L(\mathbf{R},\mathbf{R}',\mathbf{k}_1,\mathbf{k}_2)=(\gamma/\tau)\mathcal{D}(\mathbf{R},\mathbf{R}')$, where

$$\mathcal{D}(\mathbf{R},\mathbf{R}')\equiv\int_{\mathbf{K}}\sum_{n=-\infty}^{\infty}(e^{i\mathbf{K}\cdot(\mathbf{R}-\mathbf{R}_n')}-e^{i\mathbf{K}\cdot(\mathbf{R}-\mathbf{R}_n^*)})\mathcal{D}(\mathbf{K},0) =\frac{1}{4\pi D}\sum_n\left[\frac{1}{|\mathbf{R}-\mathbf{R}_n'|}-\frac{1}{|\mathbf{R}-\mathbf{R}_n^*|}\right] . \tag{3.15}$$

For a slab of width W bounded at $z=0$ and $z=W$, the images are located at $\mathbf{R}_n'=\mathbf{R}'+2n(W+2z_b)\hat{\mathbf{z}}$ and $\mathbf{R}_n^*=\mathbf{R}'-2(\mathbf{R}'\cdot\hat{\mathbf{z}}+z_b)\hat{\mathbf{z}}+2n(W+2z_b)\hat{\mathbf{z}}$. In the case of a semi-infinite medium, only the $n=0$ term is required. (By application of the Poisson resummation formula the sum over the infinite set of images leads to an equivalent expression for $\mathcal{D}$ in which the integral $\int_{\mathbf{K}}$ is replaced by a discrete sum in the direction perpendicular to the slab.) In an absorbing medium, Eq. (3.10) becomes

$$Q(\mathbf{K})\simeq 1-\frac{l}{l_i}-\frac{1}{3}l^2K^2 , \tag{3.16}$$

and thus the singular behavior of L and C in Eqs. (3.11) and (3.12) is removed

$$L=\frac{3\gamma}{l^2k^2+l^2/\xi^2},\quad C=\frac{3\gamma(1-l/l_i)}{l^2s^2+l^2/\xi^2} . \tag{3.17}$$

As discussed in Sec. II the diffusion propagator acquires an exponential decay with length $\xi\equiv(ll_i/3)^{1/2}$. The function $\mathcal{D}$ in Eq. (3.15) must then be modified by

$$\frac{1}{|\mathbf{R}-\mathbf{R}'|}\rightarrow\frac{e^{-|\mathbf{R}-\mathbf{R}'|/\xi}}{|\mathbf{R}-\mathbf{R}'|} . \tag{3.18}$$

The vertex part $C(\mathbf{R}_1,\mathbf{R}_2,\mathbf{r}_1,\mathbf{r}_2)$ describes the interference of multiple-scattering paths between points $\mathbf{R}_1\pm\mathbf{r}_1/2$ and $\mathbf{R}_2\pm\mathbf{r}_2/2$, which must lie within the scattering medium (denoted by Ω). In the diffusion approximation, and with the boundary conditions of the slab, this scattering is described by the propagator $\mathcal{D}$ in Eq. (3.15). Thus from Eq. (3.12) we are lead to the following identification:[11]

$$C(\mathbf{R}_1,\mathbf{R}_2,\mathbf{k}_1,\mathbf{k}_2)=\delta(\mathbf{R}_1-\mathbf{R}_2)\frac{\gamma(1-l/l_i)}{\tau}\int_{\mathbf{r}}e^{-i(\mathbf{k}_1+\mathbf{k}_2)\cdot\mathbf{r}}\mathcal{D}\left[\mathbf{R}_1+\frac{\mathbf{r}}{2},\mathbf{R}_1-\frac{\mathbf{r}}{2}\right] , \tag{3.19}$$

where the integral over $\mathbf{r}$ is restricted so that $\mathbf{R}_1\pm\mathbf{r}/2$ lies within the medium. The δ function comes from the in-

dependence of C on $\mathbf{K}$. Assuming normal incidence ($\hat{\mathbf{k}}_i=\hat{\mathbf{z}}$), and for backscattering into a wave-vector $\mathbf{k}_f$ differing by a small angle θ from $-\mathbf{k}_i$, the reflected intensity as a function of θ becomes

$$J(\theta)\sim I(0,\xi)+(1-l/l_i)I(\theta,\xi)\ , \tag{3.20}$$

where

$$I(\theta,\xi)\equiv\frac{1}{2\pi l^3}\int_0^W dz_+\int_0^W dz_-\, e^{-z_+/l_t}e^{-z_-/l_t}\int_\rho d^2\rho\, e^{-i\rho\cdot\mathbf{q}}\sum_n\left[\frac{e^{-(\rho^2+a_n^2)^{1/2}/\xi}}{(\rho^2+a_n^2)^{1/2}}-\frac{e^{-(\rho^2+b_n^2)^{1/2}/\xi}}{(\rho^2+b_n^2)^{1/2}}\right]. \tag{3.21}$$

Here, $\mathbf{q}\equiv\mathbf{k}_i+\mathbf{k}_f$. The mean free path l_t accounts for elastic as well as inelastic scattering

$$\frac{1}{l_t}=\frac{1}{l}+\frac{1}{l_i}\ . \tag{3.22}$$

We have made a change of variables to $z_\pm=z_1\pm z/2$, and $\boldsymbol{\rho}=(x,y)$, where $\mathbf{R}_1=(x_1,y_1,z_1)$ and $\mathbf{r}=(x,y,z)$ in Eqs. (3.13) and (3.19). This allows both the isotropic and coherent portions of Eq. (3.20) to be described by the same function $I(\theta,\xi)$. For small θ, we may write $\mathbf{q}=k_0\sin\theta\hat{\mathbf{x}}$ without loss of generality. The sum over images requires that $a_n=z_+-z+2n(W+2z_b)$ and $b_n=z_++z_-+2z_b+2n(W+2z_b)$. Evaluation of the integrals (3.21) is described in Appendix B. The resulting line shapes for various values of the width W and absorption parameter ξ are depicted in Figs. 2(a) and 2(b).

IV. ELECTROMAGNETIC WAVES: THE EFFECTS OF FARADAY ROTATION AND NATURAL OPTICAL ACTIVITY

We now extend the scalar calculation to include polarization effects.[11,13] The electric vector field E_i satisfies the wave equation and transversality condition

$$\nabla^2E_i+\frac{\omega^2}{c^2}(D_i)=j_i,\quad \nabla\cdot\mathbf{E}=0\ . \tag{4.1}$$

The displacement vector $\mathbf{D}$ is related to $\mathbf{E}$ by the dielectric tensor ϵ

$$\mathbf{D}=\epsilon\mathbf{E}=\epsilon_{\rm diag}\mathbf{E}+i\mathbf{g}\times\mathbf{E}\ . \tag{4.2}$$

We assume no dissipation ($\epsilon''=0$) and that the disorder is in the diagonal part of ϵ

$$\epsilon_{ij}=(1+\epsilon')\delta_{ij}-ie_{ijk}g_k\ , \tag{4.3}$$

where ϵ' fluctuates randomly with mean 0 and distribution given by Eq. (3.2) and e_{ijk} denotes the antisymmetric tensor. The vector $\mathbf{g}$ is the gyration vector, which in the presence of the Faraday effect is proportional to the magnetic field ($\mathbf{g}=f\mathbf{B}$), while in the case of natural optical activity it is directed along the photon wave vector ($\mathbf{g}=f\hat{\mathbf{k}}$). The averaged one-photon retarded Green's function is given by

$$G_{ij}^R(\mathbf{k})=\sum_{\alpha=\pm1}P_{ij}^\alpha(\hat{\mathbf{k}})G^\alpha(\mathbf{k})\ , \tag{4.4}$$

where

$$P_{ij}^\pm(\hat{\mathbf{k}})=\tfrac{1}{2}(\delta_{ij}-\hat{\mathbf{k}}_i\hat{\mathbf{k}}_j\mp ie_{ijm}\hat{\mathbf{k}}_m)$$

are projection matrices onto right- and left-hand circularly-polarized components which ensure that the wave is transverse. Also $[G^\pm(\mathbf{k})]^{-1}=(1\mp\hat{\mathbf{k}}\cdot\mathbf{g})k_0^2-k^2+ik_0/l$ includes the different indices of refraction for R and L polarizations. We again denote the two circular polarizations by greek indices $\alpha=\pm1$. The propagation of the field is described as before:

$$\langle E_i(\mathbf{r})\rangle=\int_{\mathbf{r}}G_{ik}^R(\mathbf{r}-\mathbf{r}')j_k(\mathbf{r}')\ . \tag{4.5}$$

Similarly the specific intensity at $\mathbf{R}$ with wave-vector $\mathbf{k}$ is

$$\begin{aligned}J_{ij}(\mathbf{R},\mathbf{k})&\equiv\int_{\mathbf{r}}e^{-\mathbf{k}\cdot\mathbf{r}}\left\langle E_i\left[\mathbf{R}+\frac{\mathbf{r}}{2}\right]E_j^*\left[\mathbf{R}-\frac{\mathbf{r}}{2}\right]\right\rangle\\&=\int_{\mathbf{R}',\mathbf{r},\mathbf{r}',\mathbf{k}'}e^{-i\mathbf{k}\cdot\mathbf{r}}e^{i\mathbf{k}'\cdot\mathbf{r}'}\left\langle G_{ik}^R\left[\mathbf{R}+\frac{\mathbf{r}}{2},\mathbf{R}'+\frac{\mathbf{r}'}{2}\right]G_{lj}^A\left[\mathbf{R}'-\frac{\mathbf{r}'}{2},\mathbf{R}-\frac{\mathbf{r}}{2}\right]\right\rangle J_{kl}^0(\mathbf{R}',\mathbf{k}')\ ,\end{aligned} \tag{4.6}$$

where J_{kl}^0 is the incident intensity. The correlation Γ_{ijkl} is now tensor valued

$$\Gamma_{ijkl}=\langle G_{ik}^RG_{lj}^A\rangle\cong\Gamma_{ijkl}^0+\int_{\mathbf{R}_1,\mathbf{R}_2,\mathbf{r}_1,\mathbf{r}_2}\Gamma_{iji'j'}^0\Lambda_{i'j'k'l'}\Gamma_{k'l'kl}\ , \tag{4.7}$$

where repeated indices are summed over, and where we have omitted the spatial arguments, which are the same as in Eq. (3.8). We perform the transformations of Eq. (3.9) and approximate the vertex as before:

$$\Lambda_{ijkl}(\mathbf{K},\mathbf{k},\mathbf{k}')=L_{ijkl}(\mathbf{K},\mathbf{k},\mathbf{k}')+C_{ijkl}(\mathbf{K},\mathbf{k},\mathbf{k}')\ , \tag{4.8}$$

where L and C refer to the ladder and maximally crossed sums, respectively. These diagrams are shown in Fig. 5(b). The solid lines refer to the Green's functions $G^{R/A}$, and the dashed lines denote scattering events. For disorder characterized by Eq. (3.2), these dashed lines contribute a (constant) factor of γ in momentum

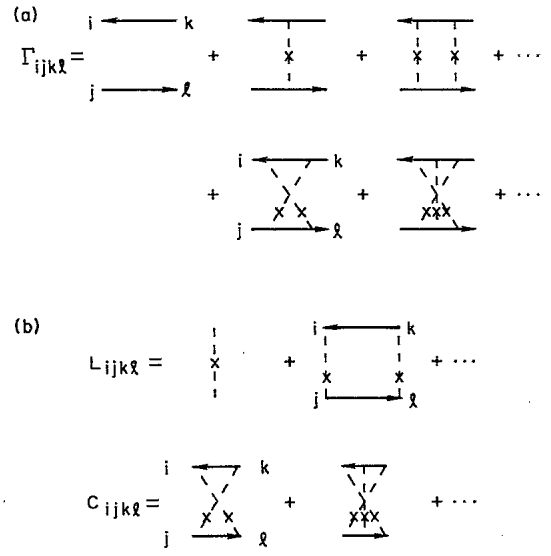

FIG. 5. The correlation $\Gamma_{ijkl}=\langle G^R_{ik}G^A_{lj}\rangle$ can be evaluated by the sum of diagrams in (a). The solid lines denote the Green's functions $G^{R/A}$ with the labeled indices and the dashed lines represent scattering. In the white-noise approximation of the disorder, these dashed lines carry a constant factor (γ) in momentum space. The principal contributions for $k_0 l \gg 1$ to Γ involve the ladder L and maximally crossed diagrams C, which may be evaluated by the sums in (b). The first term in the sum for L corresponds to single scattering and does not contribute to the helicity-preserving intensity.

space.[24] The second term of the ladder sum in Fig. 5(b), for example, represents the integral $\gamma Q_{ijkl}(\mathbf{K})$, where

$$Q_{ijkl}(\mathbf{K})=\gamma\int_{\mathbf{q}} G^R_{ik}\left[\mathbf{q}+\frac{\mathbf{K}}{2}\right]G^A_{lj}\left[\mathbf{q}-\frac{\mathbf{K}}{2}\right]$$

$$=\sum_{\alpha,\beta}Q^{\alpha\beta}_{ijkl}(\mathbf{K}) \tag{4.9}$$

and

$$Q^{\alpha\beta}_{ijkl}(\mathbf{K})\equiv\gamma\int_{\mathbf{q}} P^{\alpha}_{ik}P^{\beta}_{lj}G^{\alpha}\left[\mathbf{q}+\frac{\mathbf{K}}{2}\right]\left[G^{\beta}\left[\mathbf{q}-\frac{\mathbf{K}}{2}\right]\right]^{*} . \tag{4.10}$$

The ladder diagrams then take the form of a geometric series in the matrix $Q_{ijkl}(\mathbf{K})$. The sum is simply given by the inverse of the matrix $(1-Q)_{ijkl}$, where (ij) and (kl) are composite indices, and $1_{ijkl}=\delta_{ik}\delta_{jl}$ is the identity

$$L_{ijkl}(\mathbf{K})=\gamma\{[1-Q(\mathbf{K})]^{-1}\}_{ijkl} . \tag{4.11}$$

The inverse is obtained by first diagonalizing Q as follows.

For $K=g=0$, the matrix $Q^{\alpha\beta}$ becomes

$$Q^{\alpha\beta}_{ijkl}(0)=\langle P^{\alpha}_{ik}(\hat{\mathbf{q}})P^{\beta}_{lj}(\hat{\mathbf{q}})\rangle_{\hat{\mathbf{q}}}\gamma\int_{\mathbf{q}}|G(q)|^2 , \tag{4.12}$$

where $\langle\ \rangle_{\hat{\mathbf{q}}}$ denotes the average over the unit vector $\hat{\mathbf{q}}$ on the unit sphere. The integral over $\mathbf{q}$ has been evaluated in Appendix A with the result

$$\gamma\int_{\mathbf{q}}|G(q)|^2=\tfrac{3}{2} . \tag{4.13}$$

Upon performing the average over $\hat{\mathbf{q}}$, we have

$$Q^{\alpha\beta}_{ijkl}(0)=\tfrac{1}{40}[6\delta_{ik}\delta_{jl}+(1+5\alpha\beta)\delta_{ij}\delta_{kl}$$
$$+(1-5\alpha\beta)\delta_{il}\delta_{jk}] . \tag{4.14}$$

The nine eigenvectors of $Q^{\alpha\beta}(0)$ are independent of α and β and are the same as those of Q in Ref. 13

$$|kl\rangle_1=\frac{1}{\sqrt{3}}\delta_{kl} ,$$
$$|kl\rangle_{2,3}=\frac{1}{\sqrt{3}}\delta_{kl}e^{\pm i(l-1)2\pi/3} ,$$
$$|kl\rangle_{4,5,6}=\frac{1}{\sqrt{2}}(\delta_{ka}\delta_{lb}+\delta_{kb}\delta_{la})\quad(a\neq b) , \tag{4.15}$$
$$|kl\rangle_{7,8,9}=\frac{1}{\sqrt{2}}(\delta_{ka}\delta_{lb}-\delta_{kb}\delta_{la}) .$$

For the final six eigenvectors the spatial indices (a,b) take on the values (1,2), (1,3), and (2,3). The eigenvalues λ_m $(m=1,\ldots,9)$ of Q may be found by expanding the Green's functions about $K=0$. We show in Appendix A that these eigenvalues, for $g=0$, are given by $\lambda_m=\sum_{\alpha,\beta}\lambda^{\alpha\beta}_m$, where

$$\lambda^{\alpha\beta}_1=\left[\frac{1}{4}+\frac{\alpha\beta}{4}\right]-\frac{l^2}{4}\left[\frac{1}{3}+\frac{\alpha\beta}{3}\right]K^2 ,$$
$$\lambda^{\alpha\beta}_{2,3}=\left[\frac{7}{40}-\frac{5\alpha\beta}{40}\right]-\frac{l^2}{4}\left[\frac{7}{30}-\frac{\alpha\beta}{6}\right]K^2 ,$$
$$\lambda^{\alpha\beta}_{4,5,6}=\left[\frac{7}{40}-\frac{5\alpha\beta}{40}\right]$$
$$-\frac{l^2}{4}\left[\frac{23}{70}K^2-\frac{10}{70}(K_a^2+K_b^2)-\frac{\alpha\beta}{10}(K^2+2K_c^2)\right] \tag{4.16}$$
$$(c\neq a,b) ,$$
$$\lambda^{\alpha\beta}_{7,8,9}=\left[\frac{1}{8}+\frac{\alpha\beta}{8}\right]-\frac{l^2}{4}\left[\frac{3}{10}K^2-\frac{2}{10}(K_a^2+K_b^2)\right.$$
$$\left.+\frac{\alpha\beta}{10}(K^2-2K_c^2)\right] .$$

Here the indices a and b are distinct from each other and from c, which takes on the values 3, 2, and 1. Eq. (4.11) then becomes

$$L_{ijkl}(\mathbf{K})=\gamma\sum_{m=1}^{9}|ij\rangle_m\frac{1}{1-\lambda_m(\mathbf{K})}\langle kl|_m . \tag{4.17}$$

We note that $\lambda_1(K)=1-\frac{1}{3}l^2K^2$ corresponds to a Goldstone mode[28] since $1-\lambda_1(0)=0$. This is the origin of long-range diffusion.

The sum of maximally crossed diagrams may be found, as in the scalar case, by reversing the advanced Green's functions.[25] This transformation exchanges the indices j and l and requires time-reversal symmetry $[G^{\alpha}(-\mathbf{q})=G^{\alpha}(\mathbf{q})]$, which is violated by the Faraday

effect. In fact $G^{\alpha}(-\mathbf{q})=G^{-\alpha}(\mathbf{q})$ in this case. This is equivalent to the observation of Sec. II that, to ensure the equality of the optical path lengths of a given path and its reverse, the helicities of corresponding intermediate states in Fig. 4 must be chosen to be opposite for Faraday rotation, and must be chosen to be equal in the case of optical activity. The geometric series for C is obtained in this manner. The first term for C in Fig. 5(b), for example, represents the integral $\gamma\tilde{Q}_{ilkj}(\mathbf{s})$, where

$$\tilde{Q}_{ilkj}(\mathbf{s})=\sum_{\alpha,\beta}\tilde{Q}^{\alpha\beta}_{ilkj}(\mathbf{s}) \tag{4.18}$$

and

$$\tilde{Q}^{\alpha\beta}_{ilkj}(\mathbf{s})=\gamma\int_{\mathbf{q}}P^{\alpha}_{ik}P^{\beta}_{lj}G^{\alpha}\left[\mathbf{q}+\frac{\mathbf{s}}{2}\right][G^{\pm\beta}(\mathbf{q}-\mathbf{s}/2)]^{*} . \tag{4.19}$$

The "+" and "−" superscripts refer to the relevant interference diagrams for optical activity and Faraday rotation, respectively. In Appendix A it is shown that if $\alpha=\beta$, then $Q^{\alpha\beta}$ is independent of the gyration vector g through order g^2. For $\alpha\neq\beta$ however, g enters via the substitution $\mathbf{K}\rightarrow\mathbf{K}+\alpha k_0\mathbf{g}$ in Eq. (4.10). In particular, the eigenvalue λ_1 of Q is unaffected by both Faraday rotation and optical activity. Hence the long-range diffusion is maintained in the ladder contribution. From Eqs. (4.10) and (4.19), we see that $Q^{\alpha\beta}_{ijkl}(\mathbf{s})=\tilde{Q}^{\alpha\beta}_{ilkj}(\mathbf{s})$ in the absence of Faraday rotation. Thus the eigenvalues of $\tilde{Q}^{\alpha\beta}$ [denoted by $\kappa^{\alpha\beta}_{m}(\mathbf{s})$] are precisely those of Eq. (4.16), with the correspondence $\mathbf{K}\leftrightarrow\mathbf{s}$. In the presence of Faraday rotation, the previous analysis regarding $Q^{\alpha\beta}$ leads us to conclude that the eigenvalues $\kappa^{\alpha\beta}_{l}$ are unaffected for $\alpha\neq\beta$, and are modified by $\mathbf{s}\rightarrow\mathbf{s}+\alpha k_0\mathbf{g}$ for $\alpha=\beta$. After summing over α and β we obtain the eigenvalues

$$\begin{aligned}
&\kappa_1=1-l^2\tfrac{1}{3}(s+g^2k_0^2) ,\\
&\kappa_{2,3}=\tfrac{7}{10}-l^2\tfrac{1}{30}(7s^2+g^2k_0^2) ,\\
&\kappa_{4,5,6}=\tfrac{7}{10}-l^2[\tfrac{1}{70}(23s^2+3g^2k_0^2)\\
&\qquad\qquad -\tfrac{1}{70}(10s_a^2+10s_b^2+2g_c^2k_0^2)] ,\\
&\kappa_{7,8,9}=\tfrac{1}{2}-l^2[\tfrac{1}{10}(3s^2+g^2k_0^2)-\tfrac{2}{10}(s_a^2+s_b^2)] ,
\end{aligned} \tag{4.20}$$

where again (a,b,c) represent permutations of the spatial indices (1,2,3). The elimination of the zero eigenvalue $[1-\kappa_1(\mathbf{s})]$ of $(1-\tilde{Q})$ has the effect of rounding off the sharp backscattering peak, which comes from long diffusion paths. The sum $C_{ijkl}(\mathbf{s})$ is then obtained as for the ladder diagrams

$$\begin{aligned}
C_{ijkl}(s)&=\gamma\tilde{Q}_{ilk'j'}[(1-\tilde{Q})^{-1}]_{k'j'kj}\\
&\simeq\gamma\sum_{m=1}^{9}|il\rangle_m\frac{\kappa_m(0)}{1-\kappa_m(\mathbf{s})}\langle kj|_m .
\end{aligned} \tag{4.21}$$

The backscattered intensity may be found by generalizing Eq. (3.13)

$$\begin{aligned}
J_{ij}(\mathbf{R},\mathbf{k}_f)=&\int_{\mathbf{R}_1,\mathbf{R}_2,\mathbf{k}_1,\mathbf{k}_2}\Gamma^0_{iji'j'}(\mathbf{R}-\mathbf{R}_1,\mathbf{k}_f,\mathbf{k}_1)[L_{i'j'k'l'}(\mathbf{R}_1,\mathbf{R}_2,\mathbf{k}_1,\mathbf{k}_2)+C_{i'j'k'l'}(\mathbf{R}_1,\mathbf{R}_2,\mathbf{k}_1,\mathbf{k}_2)]\\
&\times\int_{\mathbf{R}'\in S}\Gamma^0_{k'l'kl}(\mathbf{R}_2-\mathbf{R}',\mathbf{k}_2,\mathbf{k}_i)J^0_{kl}(\mathbf{R}',\mathbf{k}_i) ,
\end{aligned} \tag{4.22}$$

where $J^0_{kl}\sim\hat{\mathbf{E}}^0_k(\hat{\mathbf{E}}^0_l)^*$ is the incident light with polarization vector $\hat{\mathbf{E}}^0$. The reflected light then has polarization vector $\hat{\mathbf{E}}$, where $J_{ij}\sim\hat{\mathbf{E}}_i(\hat{\mathbf{E}}_j)^*$. The generalization of Eq. (3.14) is just

$$\Gamma^0_{ijkl}(\mathbf{R},\mathbf{k},\mathbf{k}')\simeq\sum_{\alpha,\beta}P^{\alpha}_{ik}(\hat{\mathbf{k}})P^{\beta}_{lj}(\hat{\mathbf{k}})\Gamma^0(\mathbf{R},\mathbf{k},\mathbf{k}')=\delta_{ik}(\hat{\mathbf{k}})\delta_{lj}(\hat{\mathbf{k}})\Gamma^0(\mathbf{R},\mathbf{k},\mathbf{k}') , \tag{4.23}$$

where $\delta_{ij}(\hat{\mathbf{k}})=\delta_{ij}-\hat{\mathbf{k}}_i\hat{\mathbf{k}}_j$.

Recently experiments have been carried out in which circularly-polarized light is incident (say along $\hat{\mathbf{k}}_i\equiv\hat{\mathbf{z}}$), and only light of the same polarization (say along $\hat{\mathbf{k}}_f\simeq-\hat{\mathbf{k}}_i$) is observed.[18] This is what we refer to as the helicity-preserving channel. It may be obtained from Eq. (4.22) with $\hat{\mathbf{E}}^0=(1/\sqrt{2})(1,i,0)$, and by projecting out the right-hand portion of J. Since $\hat{\mathbf{E}}_i\hat{\mathbf{E}}^*_j=P^{+}_{ij}(\hat{\mathbf{k}})$ for a right-hand wave traveling in the $\hat{\mathbf{k}}$ direction, and since $P^{+}_{ji}P^{+(-)}_{ij}=1(0)$, this projection may be obtained with P^{+}

$$J^{+}(\mathbf{k}_f)\equiv P^{+}_{ji}(\hat{\mathbf{k}}_f)J_{ij}(\mathbf{k}_f) . \tag{4.24}$$

We evaluate the coherent backscattering portion of this in Appendix B. The result is

$$\begin{aligned}
J^{+}_{\mathrm{coh}}\sim&\left[1-\frac{(lk_0g)^2}{3}\right]I\left[\theta,\frac{1}{k_0g}\right]+\tfrac{1}{2}\left[1-\frac{(lk_0g)^2}{21}\right]I\left[\theta,l\left[\frac{7}{9+(lk_0g)^2}\right]^{1/2}\right]\\
&-\tfrac{5}{6}\left[1-\frac{(lk_0g)^2}{5}\right]I\left[\theta,l\left[\frac{3}{5+(lk_0g)^2}\right]^{1/2}\right] ,
\end{aligned} \tag{4.25}$$

where $I(\theta,\xi)$ is defined in Eq. (3.21). In this channel, the incoherent portion of the scattered light should have no contributions from single pointlike scattering events, since such would necessarily flip the helicity. If one writes $1/(1-\lambda_m)$ in Eq. (4.17) as $1+\lambda_m/(1-\lambda_m)$, then the leading 1 corresponds to single-scattering events. These are represented by the first term in Fig. 5(b). One finds that, indeed, in the helicity-preserving channel, the terms in the intensity arising from such events cancel exactly. Because of this elimination of single-scattering terms, the resulting peak has a height at $\theta=0$ of exactly twice the incoherent background—as is true for scalar waves.[11,12] This is in contrast with the parallel polarized case, where this ratio is somewhat less than two.[13] Furthermore, the approximate cancellation between the second and third terms in Eq. (4.25) leads to the fact that the backscattering peak in this channel closely resembles the calculated scalar line shape. This similarity persists in the presence of absorption and Faraday rotation, since the first term in Eq. (4.25) is precisely the coherent portion of the scalar result of Eq. (3.20) with the correspondence $\xi\leftrightarrow(gk_0)^{-1}$—compare Figs. 2(b) and 3(a). At this point, another claim made in Sec. II may be clarified. Consider the paths shown in Fig. 4 (in the absence of Faraday rotation). The path shown contributing to the helicity-preserving channel corresponds to a product $Q^{\alpha_1\alpha_1}\cdots Q^{\alpha_N\alpha_N}$, while the path (with helicities labeled in parentheses) contributing to the opposite helicity channel corresponds to a product $Q^{\alpha_1,-\alpha_1}\cdots Q^{\alpha_N,-\alpha_N}$. Long paths are associated with the eigenvalue λ_1 (the Goldstone mode). Thus, since $\lambda_1^{\alpha,-\alpha}=0$, long paths of the second type are suppressed. Only short paths, corresponding to eigenvalues $\lambda_{2,\ldots,9}^{\alpha,-\alpha}$, contribute to the opposite helicity channel.

In an optically active medium, the rotatory power f affects only the eigenvalues $\lambda_m^{\alpha,-\alpha}(\mathbf{K})$ and $\kappa_m^{\alpha,-\alpha}(\mathbf{s})$, since time-reversal symmetry is maintained. (These eigenvalues are, in fact, equal with the identification $\mathbf{K}\leftrightarrow\mathbf{s}$.) The eigenvalues $\kappa_m(\mathbf{s})$ are derived in Appendix A

$$\begin{aligned}
\kappa_1&=1-l^2\tfrac{1}{3}s^2\,,\\
\kappa_{2,3}&=\tfrac{7}{30}-l^2\tfrac{1}{30}(7s^2+18f^2k_0^2)\,,\\
\kappa_{4,5,6}&=\tfrac{7}{10}-l^2[\tfrac{1}{70}(23s^2+42f^2k_0^2)\\
&\qquad-\tfrac{1}{70}(10s_a^2+10s_b^2)]\,,\\
\kappa_{7,8,9}&=\tfrac{1}{2}-l^2[\tfrac{3}{10}s^2-\tfrac{2}{10}(s_a^2+s_b^2)]\,.
\end{aligned}\tag{4.26}$$

We see that Goldstone mode is preserved. Hence, the sharp backscattering peak in the helicity-preserving channel remains. It is the opposite helicity channel which is suppressed by the optical activity [see Fig. 3(b)].

V. DISCUSSION

Previous discussions of the polarization effects in coherent backscattering have dealt with linearly polarized light.[4,5,13] In this presence of Faraday rotation or optical activity it is clearly more natural to consider circularly-polarized light. Furthermore, for incident light of a given circular polarization, we have shown that the intensity of scattered light of the same circular polarization yields an angular profile closely resembling the calculated scalar line shape. This has been seen recently in experimental line shapes obtained by Etemad *et al.*, in which precisely this helicity-preserving channel was monitored.[18] These line shapes are consistent with the scalar calculations depicted in Figs. 2(a) and 2(b). This is in contrast with the case of parallel linearly polarized light, for which the intensity differs from the scalar result by a rather large correction term[13]—compare Figs. 2(b) and 6. The intensity in the helicity-preserving channel given by Eq. (4.25), however, involves a destructive interference between correction terms which are added to the scalar line shape.

We have demonstrated an exact factor of 2 enhancement of the backscattering peak in the helicity-preserving channel, which is the same as for scalar waves. This factor of 2 enhancement is a consequence of time-reversal symmetry relating the ladder diagrams (contributing to the incoherent intensity) to the maximally crossed diagrams (contributing to the coherent peak). This symmetry, in fact, relates *arbitrary* diagrams contributing to the coherent and incoherent portions of the scattered light—with the exception of the single-scattering (ladder) diagram of Fig. 5(b). For scalar waves, the singular nature of the ladder and maximally crossed sums makes this first diagram irrelevant for small $\mathbf{K}$ and $\mathbf{k}+\mathbf{k}'$ [see Eq (3.12)]. In the helicity-preserving channel for vector waves, the contributions from this first diagram cancel. (This is equivalent to the observation that single-scattering events do not preserve helicity.[18]) Thus, in the helicity-preserving channel, as for scalar waves, an exact factor of 2 enhancement is obtained. For parallel polarized light, however, the single-

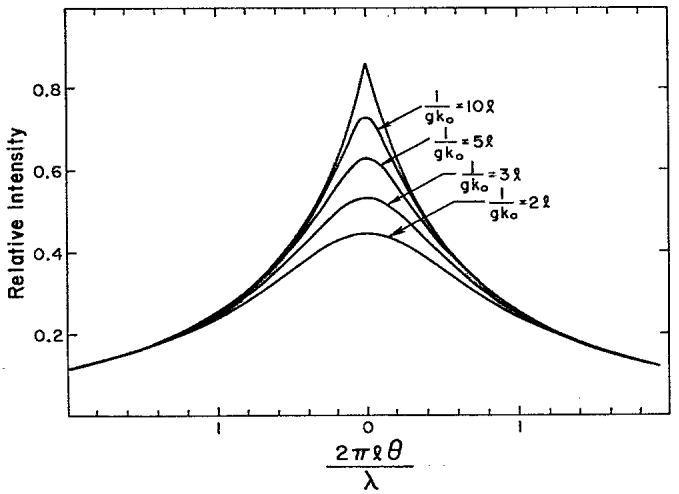

FIG. 6. The effect of Faraday rotation on the peak intensity of light polarized parallel to the incident wave. In the presence of time-reversal symmetry, the enhancement factor at $\theta=0$ is somewhat less than 1.9—we have normalized by the isotropic background in this channel. Also, the suppression of the peak due to time-reversal symmetry breaking is less severe than in the helicity-preserving channel or for scalar waves.

scattering diagram increases the incoherent portion of the scattered light—reducing the enhancement factor to about 1.87,[13] as seen in recent experiments.[15,19]

By examining the effects of Faraday rotation on the coherent backscattering peak, one sees more clearly the role of time-reversal symmetry. Geometric constraints and absorption lead simply to a truncation of long diffusion paths—suppressing both the coherent peak and the incoherent portions of the reflected intensity. Faraday rotation, on the other hand, suppresses only the peak portion of the reflected light in the helicity-preserving channel. Parity nonconservation has not previously been examined in the context of localization. We have shown that parity nonconservation due to optical activity has no discernible effect on the helicity-preserving component of the peak intensity, but rather suppresses only the broader reversed helicity component. In terms of the parameters in Figs. 3(a) and 3(b), $\frac{1}{2}gk_0l$ and $\frac{1}{2}fk_0l$ describe the amount of rotation (in radians) of the plane of polarization over one mean free path. Thus for a mean free path of about 20 μm, a rotation of as much as 500° per mm is required for the effects of Faraday rotation and optical activity on the line shape to be observable. In real materials, such strong Faraday rotation will be accompanied by absorption. Thus, in experiments care must be taken to distinguish between these effects, which have similar consequences for the helicity-preserving channel. Such rotatory powers are more easily attainable, however, in some optically active materials.[21] The breakdown of both time-reversal and parity symmetries may have interesting consequences in the localization critical region. Faraday rotation and optical activity provide possible probes with which the roles of these symmetries may be studied in photon localizing systems.

In this work we have assumed a white-noise approximation, in which the disorder is spatially uncorrelated. This suffices to describe well the features so far observed in coherent backscattering experiments. This approximation, however, will cease to be valid near scattering resonances due to large particles or near a mobility edge. The importance of spatial correlations has been observed experimentally[29] in titania microstructures for which $l \lesssim \lambda$. Thus, we cannot expect the model of uncorrelated disorder to yield a sufficient description of the strong localization of photons. It has been suggested recently that large scale geometric resonances may play an important role in observing strong localization of light.[30] In particular, in suitably prepared dielectric superlattices with moderate disorder, photons may become localized within a narrow frequency range. Due to Bragg resonances of the underlying lattice, the allowed wave-vectors $\mathbf{k}$ for photon propagation may be severely restricted for frequencies near a band edge. Thus intermediate states in coherent backscattering paths will be restricted—perhaps leading to observable features in the coherent line shape. To understand quantitatively any of the effects of spatially correlated disorder on the localization of photons, however, it will be necessary to go beyond the approximations of the present work.[31]

ACKNOWLEDGMENTS

This work was supported by the National Science Foundation (NSF) under Grant No. DMR-85-18163. One of the authors (F.M.) also wishes to thank the NSF for financial support.

APPENDIX A

In the following we describe the evaluation of $Q^{\alpha\beta}_{ijkl}(\mathbf{K})$ and the eigenvalues $\lambda^{\alpha\beta}_{1,\ldots,9}(\mathbf{K})$. This is done first in the absence of Faraday rotation and optical activity. Then we show how the matrices $Q^{\alpha\beta}$ and $\tilde{Q}^{\alpha\beta}$ are altered in the presence of these effects.

We begin with Eq. (4.10)

$$Q^{\alpha\beta}_{ijkl}(\mathbf{K})=\gamma\int_{\mathbf{q}} P^{\alpha}_{ik}P^{\beta}_{lj}G^{\alpha}\left[\mathbf{q}+\frac{\mathbf{K}}{2}\right]\left[G^{\beta}\left[\mathbf{q}-\frac{\mathbf{K}}{2}\right]\right]^{*} . \tag{A1}$$

We separate the integral over $\mathbf{q}$ into an integral over $q=|\mathbf{q}|$ and an average over $\hat{\mathbf{q}}$. It is sufficient to find the eigenvalues for $Kl \ll 1$. Since $1 \ll k_0 l \sim ql$, we may take $\hat{\mathbf{q}}$ as the argument of the projection matrices I^{α} and P^{β}

$$Q^{\alpha\beta}_{ijkl}(\mathbf{K})=4\pi\gamma\left\langle P^{\alpha}_{ik}(\hat{\mathbf{q}})P^{\beta}_{lj}(\hat{\mathbf{q}})\frac{1}{(2\pi)^3}\int_0^{\infty} q^2dq\, G\left[\mathbf{q}+\frac{\mathbf{K}}{2}\right]G^{*}\left[q-\frac{\mathbf{K}}{2}\right]\right\rangle_{\hat{\mathbf{q}}} . \tag{A2}$$

An expansion of the Green's functions about $K=0$ yields the following integrand:

$$q^2G\left[\mathbf{q}+\frac{\mathbf{K}}{2}\right]G^{*}\left[\mathbf{q}-\frac{\mathbf{K}}{2}\right]\simeq q^2GG^{*}\left[1+(\mathbf{q}\cdot\mathbf{K})^2[G^2+(G^{*})^2-GG^{*}]_1+\frac{K^2}{4}[G+G^{*}]_2\right] , \tag{A3}$$

where the argument $(\mathbf{q})$ of the G's has been omitted. For $K=0$, Eq. (A1) reduces to Eq. (4.12), and the integral over $\mathbf{q}$ may be evaluated as follows.[13] For weak scattering, the self-energy $\Sigma=\gamma\mathrm{Tr}\int_{\mathbf{q}} G_{ij}=\frac{2}{3}\gamma\int_{\mathbf{q}} G$, where $\mathrm{Im}(\Sigma)=-\mathrm{Im}[G^{-1}(q)]$. From this, we obtain

$$\mathrm{Im}(\Sigma)=\tfrac{2}{3}\gamma\,\mathrm{Im}\int_{\mathbf{q}} G(q)\frac{G^{*}(q)}{G^{*}(q)}=\gamma\,\mathrm{Im}(\Sigma)\tfrac{2}{3}\int_{\mathbf{q}}|G(q|^2 , \tag{A4}$$

and Eq. (4.13)

$$\gamma \int_{\mathbf{q}} |G(q)|^2 = \frac{4\pi\gamma}{(2\pi)^3} \int_0^\infty dq\, q^2 G(q) G^*(q) = \tfrac{3}{2} . \quad \text{(A5)}$$

The mean free path l is related to γ by

$$l = \tfrac{3}{2} \times \frac{4\pi}{\gamma} . \quad \text{(A6)}$$

The other integrals over q, in the expansion, may be done by contour integration. For example, the term $[\ ]_2$ leads to the integral

$$\frac{2\pi\gamma}{(2\pi)^3} \int_0^\infty dq\, q^2 G(q) G^*(q) [G(q) + G^*(q)] = -\frac{3}{8k_0^2} . \quad \text{(A7)}$$

Since $k_0 l \gg 1$, however, this term leads to a contribution of lower order in $1/k_0 l$. Thus, the term $[\ ]_2$ in Eq. (A3) may be dropped. Evaluation of the integral associated with $[\ ]_1$ leads to

$$Q_{ijkl}^{\alpha\beta}(\mathbf{K}) = \tfrac{3}{2} \langle P_{ik}^{\alpha}(\hat{\mathbf{q}}) P_{lj}^{\beta}(\hat{\mathbf{q}}) (1 - \hat{\mathbf{q}}_m \hat{\mathbf{q}}_n K_m K_n) \rangle_{\hat{\mathbf{q}}} , \quad \text{(A8)}$$

from which we obtain the eigenvalues in Eq. (4.16) to leading order in K^2

$$\lambda_m^{\alpha\beta} = \langle ij \,|\, {}_m Q_{ijkl}^{\alpha\beta}(\mathbf{K}) \,|\, kl \rangle_m . \quad \text{(A9)}$$

To find the modification of $Q^{\alpha\beta}(\mathbf{K})$ and $\tilde{Q}^{\alpha\beta}(\mathbf{s})$ due to Faraday rotation, we simply write (to leading order in $1/k_0 l$)

$$G^{\alpha}(q + \tfrac{1}{2}K)[G^{\beta}(q - \tfrac{1}{2}K)]^* = \frac{1}{k_0^2 - q^2 - \alpha \mathbf{g}\cdot\hat{\mathbf{q}} k_0^2 - \mathbf{K}\cdot\mathbf{q} + ik_0/l} \frac{1}{k_0^2 - q^2 - \beta \mathbf{g}\cdot\hat{\mathbf{q}} k_0^2 + \mathbf{K}\cdot\mathbf{q} - ik_0/l} . \quad \text{(A10)}$$

If $\alpha = \beta$, the $\mathbf{g}$ may be absorbed into a redefinition of the integration variable $\mathbf{q}$. Thus $Q^{\alpha\alpha}$ and $\tilde{Q}^{\alpha,-\alpha}$, in Eqs. (A1) and (4.19) are unaltered. For $\alpha \neq \beta$, we see that Eq. (A10) is equivalent to Eq. (A3) with a redefinition: $\mathbf{K}\cdot\mathbf{q} \to \mathbf{K}\cdot\mathbf{q} + \alpha \mathbf{g}\cdot\hat{\mathbf{q}} k_0^2$. This leads to the substitution $\mathbf{K} \to \mathbf{K} + \alpha k_0 \mathbf{g}$ in Eq. (A8), since the poles are near $q = \pm k_0$. The matrix $\tilde{Q}^{\alpha\beta}$ is obtained similarly:

$$\tilde{Q}_{ilkj}^{\alpha\beta}(\mathbf{s}) = \tfrac{3}{2} \langle P_{ik}^{\alpha}(\hat{\mathbf{q}}) P_{lj}^{\beta}(\hat{\mathbf{q}}) [1 - \hat{\mathbf{q}}_m \hat{\mathbf{q}}_n (s_m + \alpha k_0 g_m)(s_n + \alpha k_0 g_n)] \rangle_{\hat{\mathbf{q}}} . \quad \text{(A11)}$$

After summing over α,β and averaging over $\hat{\mathbf{q}}$, we obtain the eigenvalues of Eq. (4.20):

$$\kappa_m^{\alpha\beta} = \langle il \,|\, {}_m \tilde{Q}_{ilkj}^{\alpha\beta}(\mathbf{s}) \,|\, kj \rangle_m . \quad \text{(A12)}$$

In the case of optical activity, both $Q^{\alpha\alpha}$ and $\tilde{Q}^{\alpha\alpha}$ are unaffected, since the Green's functions are shifted equally in frequency. On the other hand, for $\alpha \neq \beta$, we see [from Eq. (A10), with $\mathbf{g} = f\hat{\mathbf{q}}$] that $Q^{\alpha\beta}$ and $\tilde{Q}^{\alpha\beta}$ must be modified by $\mathbf{q}\cdot\mathbf{K} \to \mathbf{q}\cdot\mathbf{K} + \alpha f k_0^2$ and $\mathbf{q}\cdot\mathbf{s} \to \mathbf{q}\cdot\mathbf{s} + \alpha f k_0^2$. Thus, for example, the eigenvalues $\kappa_m(\mathbf{s})$ in Eq. (4.26) are obtained from

$$\tilde{Q}_{ilkj}^{\alpha\beta}(\mathbf{s}) = \tfrac{3}{2} \langle P_{ik}^{\alpha}(\hat{\mathbf{q}}) P_{lj}^{\beta}(\hat{\mathbf{q}}) (1 - \delta_{\alpha,-\beta} f^2 k_0^2 - \hat{\mathbf{q}}_m \hat{\mathbf{q}}_n s_m s_n) \rangle_{\hat{\mathbf{q}}} . \quad \text{(A13)}$$

APPENDIX B

We evaluate the integral (4.22) in the helicity-preserving channel. By the discussion leading up to Eq. (4.24), we may express the intensity in this channel as

$$J^+(\theta) \sim P_{ji}^+(\hat{\mathbf{k}}_f) \int \Gamma_{iji'j'}^0 [L_{i'j'k'l'} + C_{i'j'k'l'}] \Gamma_{k'l'kl}^0 P_{kl}^+(\hat{\mathbf{k}}_i)$$

$$\simeq \int \Gamma^0 P_{ji}^+(-\hat{\mathbf{z}}) [L_{ijkl} + C_{ijkl}] P_{kl}^+(\hat{\mathbf{z}}) \Gamma^0 , \quad \text{(B1)}$$

for normal incidence along $\hat{\mathbf{z}}$, and for small backscattering angle θ. We have omitted the arguments of Γ^0, L, and C as well as the limits of integration, all of which are the same as in Eqs. (3.13) and (4.22). Consider just the coherent contribution

$$J_{\text{coh}}^+ \sim \sum_{m=1}^{9} P_{ji}^+(-\hat{\mathbf{z}}) \,|\, il \rangle_m \langle kj \,|\, {}_m P_{kl}^+(\hat{\mathbf{z}}) \times \int \Gamma^0 C_m(\mathbf{R}_1, \mathbf{R}_2, \mathbf{k}_1, \mathbf{k}_2) \Gamma^0 . \quad \text{(B2)}$$

The functions C_m are obtained in the same way as was C in Eq. (3.19)

$$C_m(\mathbf{R}_1, \mathbf{R}_2, \mathbf{k}_1, \mathbf{k}_2) = \delta(\mathbf{R}_1 - \mathbf{R}_2) \frac{\gamma}{\tau} \times \int_{\mathbf{R}_1 \pm \mathbf{r}/2 \in \Omega} e^{-i(\mathbf{k}_1 + \mathbf{k}_2)\cdot\mathbf{r}} \times \mathcal{D}_m \left[\mathbf{R}_1 + \frac{\mathbf{r}}{2}, \mathbf{R}_1 - \frac{\mathbf{r}}{2} \right] , \quad \text{(B3)}$$

where

$$\mathcal{D}_m(\mathbf{R}, \mathbf{R}') \equiv \tau \int_{\mathbf{s}} \sum_n (e^{i\mathbf{s}\cdot(\mathbf{R} - \mathbf{R}_n')} - e^{i\mathbf{s}\cdot(\mathbf{R} - \mathbf{R}_n^*)}) \frac{\kappa_m(\mathbf{s})}{1 - \kappa_m(\mathbf{s})} . \quad \text{(B4)}$$

The locations of the images, $\mathbf{R}_n'$ and $\mathbf{R}_n^*$, are the same as for Eq. (3.15). (τ is the mean free time.)

The eigenvalues $\lambda_m(\mathbf{K})$ and $\kappa_m(\mathbf{s})$ are, in general, anisotropic in the variables $\mathbf{K}$ and $\mathbf{s}$. For example, the coefficient of s_c^2 differs from that of $s_{a,b}^2$ in $\kappa_{4,\ldots,9}$. We may write a general eigenvalue $\kappa_m(\mathbf{s}) = \kappa_m^0 - \kappa_m''(s_c^2 + \sigma^2 s_\perp^2) l^2$, where $\mathbf{s}_\perp = (s_a, s_b)$. By a change of variables ($\mathbf{s}_\perp \to \sigma \mathbf{s}_\perp$), the transform $\mathcal{D}_m$, in an infinite medium, becomes

$$\mathcal{D}_m(\mathbf{r}) \simeq \tau \int_{\mathbf{s}} e^{i\mathbf{s}_\perp\cdot\mathbf{r}_\perp} e^{is_c r_c} \frac{\kappa^0}{1 - \kappa^0 + \kappa''(s_c^2 + \sigma^2 s_\perp^2) l^2} = \frac{\tau}{4\pi l^2 \sigma^2} \left[\frac{\kappa^0}{\kappa''} \right] \frac{e^{-(r_c^2 + r_\perp^2/\sigma^2)^{1/2}/\xi}}{(r_c^2 + r_\perp^2/\sigma^2)^{1/2}} , \quad \text{(B5)}$$

where $\xi_m \equiv l(\kappa_m''/1-\kappa_m^0)^{1/2}$. With the boundary conditions of a slab, $\mathcal{D}_m(\mathbf{R},\mathbf{R}')$ is obtained from this by summing over the images. The only surviving projections in Eq. (B2) are

$$P_{ji}^{+}(-\hat{\mathbf{z}})\,|\,il\,\rangle_m\langle\,kj\,|\,{}_mP_{kl}^{+}(\hat{\mathbf{z}})=\begin{cases}\frac{1}{3}, & m=1\\ \frac{1}{12}, & m=2,3\\ \frac{1}{2}, & m=7\end{cases} \tag{B6}$$

where we associate $m=7$ with $a=1$, $b=2$, and $c=3$ in Eq. (4.15). By letting $\rho=\mathrm{r}_\perp/\sigma$ in Eq. (B3), the expression for the intensity as a function of θ becomes

$$J_{\mathrm{coh}}^{+}(\theta)\sim\tfrac{1}{3}\left[\frac{\kappa_1^0}{\kappa_1''}\right]I(\theta,\xi_1)+\tfrac{1}{6}\left[\frac{\kappa_2^0}{\kappa_2''}\right]I(\theta,\xi_2) -\tfrac{1}{2}\left[\frac{\kappa_7^0}{\kappa_7''}\right]I(\theta,\xi_7)\,, \tag{B7}$$

where $I(\theta,\xi)$ is given in Eq. (3.21). We have written this result in Eq. (4.25), for the case of Faraday rotation.

The integrals over $z_\pm$ in Eq. (3.21) are easily evaluated, after completing the integral over $\boldsymbol{\rho}$. The general form of this integral over $\boldsymbol{\rho}$ is

$$\int_\rho d^2\rho\, e^{-i\mathbf{q}\cdot\boldsymbol{\rho}}\times\frac{e^{-(\rho^2+a^2)^{1/2}/\xi}}{(\rho^2+a^2)^{1/2}}=\int_0^\infty d\rho\,\rho\frac{e^{-(\rho^2+a^2)^{1/2}/\xi}}{(\rho^2+a^2)^{1/2}}\times\int_0^{2\pi}d\phi\, e^{-iq\rho\cos\phi}\,. \tag{B8}$$

The integral over ϕ simply yields the Bessel function J_0

$$\int_0^{2\pi}d\phi\, e^{-iq\rho\cos\phi}=2\pi J_0(q\rho)\,. \tag{B9}$$

And by a change of variables $[r=(\rho^2+a^2)^{1/2}]$, Eq. (B8) becomes[13,32]

$$2\pi\int_{|a|}^\infty e^{-r/\xi}J_0[q(r^2-a^2)^{1/2}]dr=2\pi\frac{e^{-(q^2+1/\xi^2)^{1/2}|a|}}{(q^2+1/\xi^2)^{1/2}}\,. \tag{B10}$$

[1] S. John, Phys. Rev. Lett. **53**, 2169 (1984).
[2] P. W. Anderson, Philos. Mag. B **52**, 505 (1985).
[3] Y. Kuga and A. Ishimaru, J. Opt. Soc. Am. A **1**, 831 (1984).
[4] M. van Albada and A. Lagendijk, Phys. Rev. Lett. **55**, 2692 (1985).
[5] P. E. Wolf and G. Maret, Phys. Rev. Lett. **55**, 2696 (1985).
[6] S. Etemad, R. Thompson, and M. J. Andrejco, Phys. Rev. Lett. **57**, 575 (1986).
[7] M. Kaveh, M. Rosenbluh, I. Edrei, and I. Freund, Phys. Rev. Lett. **57**, 2049 (1986).
[8] D. E. Khmel'nitskii, Physica **126B**, 235 (1984); B. L. Al'tshuler, A. G. Aronov, D. E. Khmel'nitskii, and A. I. Larkin, in *Quantum Theory of Solids,* edited by I. M. Lifshits (Mir, Moscow, 1982), pp. 130–237.
[9] G. Bergmann, Phys. Rep. **107**, 1 (1984).
[10] E. Abrahams, P. W. Anderson, D. C. Liccardello, T. V. Ramakrishnan, Phys. Rev. Lett. **42**, 673 (1979).
[11] A. A. Golubentsev, Zh. Eksp. Teor. Fiz. **86**, 47 (1984) [Sov. Phys.—JETP **59**, 26 (1984)].
[12] E. Akkermans, P. E. Wolf, and R. Maynard, Phys. Rev. Lett. **56**, 1471 (1986).
[13] M. J. Stephen and G. Cwilich, Phys. Rev. B **34**, 7564 (1986).
[14] S. Etemad (unpublished).
[15] M. Rosenbluh, I. Edrei, M. Kaveh, and I. Freund, Phys. Rev. A **35**, 4458 (1987).
[15] K. M. Watson, J. Math. Phys. **10**, 688 (1969); D. A. de Wolf, IEEE Trans. Antennas Propag. **19**, 254 (1971); Y. Kuga, L. Tsang, and A. Ishimaru, J. Opt. Soc. Am. A **2**, 616 (1985).
[17] I. Edrei and M. Kaveh, Phys. Rev. B **35**, 6461 (1987).
[18] S. Etemad, R. Thompson, M. J. Andrejco, S. John and F. MacKintosh, Phys. Rev. Lett. **59**, 1420 (1987).
[19] A. Lagendijk (unpublished).
[20] L. D. Landau and E. M. Lifshitz, *Electrodynamics of Continuous Media* (Pergamon, New York 1960).
[21] A. Yariv and P. Yeh, *Optical Waves in Crystals* (Wiley, New York, 1984).
[22] E. U. Condon, Rev. Mod. Phys. **9**, 432 (1937).
[23] G. Cwilich and M. J. Stephen, Phys. Rev. B **35**, 6517 (1987).
[24] A. A. Abrikosov, L. P. Gor'kov, and I. E. Dzyaloshinskii, *Quantum Field Theoretical Methods in Statistical Physics* (Dover, New York, 1963).
[25] J. S. Langer and T. Neal, Phys. Rev. Lett. **16**, 984 (1965).
[26] M. P. van Albada, M. B. van der Mark, and A. Lagendijk, Phys. Rev. Lett. **58**, 361 (1987).
[27] B. Davison and J. B. Sykes, *Neutron Transport Theory* (Oxford University, New York, 1957).
[28] L. Schäfer and F. Wegner, Z. Phys. B **38**, 113 (1980); A. J. McKane and M. Stone, Ann. Phys. (N.Y.) **131**, 36 (1981); S. John, H. Sompolinsky, and M. Stephen, Phys. Rev. B **27**, 5592 (1983).
[29] A. Z. Genack, Phys. Rev. Lett. **58**, 2043 (1987).
[30] S. John, Phys. Rev. Lett. **58**, 2486 (1987).
[31] S. John and M. J. Stephen, Phys. Rev. B **28**, 6358 (1983).
[32] I. S. Gradshteyn and I. M. Ryzhik, *Table of Integrals Series and Products* (Academic, New York, 1980), Sec. 6.646.